Transport properties of hydrogen-helium mixtures at extreme density and temperature conditions

Dafang Li,[1] Cong Wang,[1,2] Wei Kang,[2] Jun Yan,[1,2] and Ping Zhang[1,2,*]

[1]*Institute of Applied Physics and Computational Mathematics, P.O. Box 8009, Beijing 100088, People's Republic of China*

[2]*Center for Applied Physics and Technology, Peking University, Beijing 100871, People's Republic of China*

(Received 14 August 2015; revised manuscript received 12 September 2015; published 22 October 2015)

We perform a systematic study of hydrogen-helium mixtures using quantum molecular dynamics (QMD) with a focus on the equations of state and structural and transport properties such as electrical conductivity, diffusion, and viscosity at conditions of giant planet interiors of $0.2 \sim 2.3$ g/cm^3 and $1000 \sim 80\,000$ K for a typical helium mass fraction of 0.245. The H-He separation is found at low temperatures by analyzing the trajectories and pair distribution functions. We show that the diffusion coefficients exhibit transitions from kinetics- to potential-, and then to demixing-dominated regimes. In addition, we identify the discontinuity feature of optical absorption of a H-He mixture at low density and temperature conditions, which results from the change from an intraband to an interband transition. The Stokes-Einstein relation between the diffusion and viscosity coefficients is also discussed.

DOI: 10.1103/PhysRevE.92.043108 PACS number(s): 52.25.Fi, 51.30.+i, 51.20.+d, 52.65.Yy

I. INTRODUCTION

Hydrogen-helium mixtures are the major constituents of the giant planets. For example, they form about 70%–95% of the mass of Jupiter and Saturn [1]. The thermodynamic and transport properties of H-He mixtures in warm dense regimes are therefore crucial for constructing the structure and dynamo models of such planets. Especially, a long-standing puzzle about the excess luminosity of Saturn has not yet been explained [2], which requires accurate equations of state (EOSs) of H-He mixtures. The electrical transport coefficients are important for locating the boundary between a nonconducting outer and a metallic inner envelope as assumed in interior models of giant planets. In addition, the viscosity and diffusion coefficients have an increasingly important effect in hot spot ignition for inertial confinement fusion (ICF), since they are now well acknowledged to be key factors for ablator materials to degrade the fuel [3,4]. Although the exploration of single species has made great progress, it is still challenging to characterize the properties of mixtures.

Experimental researches on H-He mixtures are indispensable for exploring their characteristics under extreme conditions. However, only a very few experiments have been performed for the H-He phase diagram, with the pressure-temperature state reached experimentally so far up to 30 GPa and 7000 K [5]. The properties of H-He mixtures at the higher pressure and temperature conditions of the interior of giant planets are determined mostly through theoretical modeling. The most concerned issue is H-He phase separation, which has been assumed to be responsible for the discrepancies between the observed luminosity of Saturn and the one predicted by homogeneous evolutionary models [6–8]. Since Salpeter first predicted the demixing of H-He mixtures at giant planet interior conditions [8], several theoretical studies have attempted to clarify this phenomenon and determine the demixing lines using first-principles simulation methods based on density functional theory (DFT). Using the ideal mixing approximation, Klepeis *et al.* obtained a demixing temperature of 15000 K for $x_{\mathrm{He}} = 0.07$, suggesting that there should occur phase separation in both Jupiter and Saturn [9]. Pfaffenzeller *et al.* estimated the free energies of the mixture using first-principles molecular dynamics with the Car-Parrinello technique and obtained much lower immiscibility temperatures [10]. Using a combination of DFT-based molecular dynamics together with thermodynamic integration techniques, Morales *et al.* calculated the Gibbs free energy of the dense liquid as a function of pressure, temperature, and composition, and thus predicted the immiscible regimes inside Saturn [11,12]. It is worth mentioning that these predictions represent the most accurate calculations of helium miscibility in high-pressure hydrogen to date. The results at pressures above 3 Mbar agree well with those predicted by Lorenzen *et al.* with the ideal mixing approximation for the entropy [13]. In addition, it has been proposed that reflectivity measurements could be used to identify this liquid-liquid phase transition [14]. Wang *et al.* examined the mixing rules with respect to the EOS, diffusion coefficients, and viscosity of H-He mixtures [15].

In this paper, we study systematically and in a consistent way the EOSs and structural and transport properties of H-He mixtures with typical helium mass fractions of 0.245 in extensive density and temperature regimes relevant to the interior of giant planets, with the aim of exploring the impact of H-He demixing on these properties. By analyzing the structural properties, we confirm H-He demixing at low temperatures. In combination with the Kubo-Greenwood formula, we calculate the electrical and optical properties in the next section. The locations of nonmetal-to-metal transitions are determined. And then we discuss the change of the diffusion behavior with the plasma characteristic parameter. Finally we close our paper with a summary of our main results.

II. COMPUTATIONAL METHOD

A. Quantum molecular dynamics

In the present study, the quantum molecular dynamics simulations are implemented by employing the Vienna *ab initio* simulation package (VASP) plane-wave pseudopotential code developed at the Technical University of Vienna [16,17]. Within the framework of finite-temperature (FT) DFT [18,19], the active electrons are treated in a full quantum

*Corresponding author: zhang_ping@iapcm.ac.cn

way with the electronic states populated according to the Fermi-Dirac statistics, while the ions move classically driven by the force derived via the Hellmann-Feynman theorem at each molecular dynamics (MD) step. The all-electron projector augmented wave (PAW) potentials are used to describe the interactions between the active electrons and the ions, with the exchange-correlation energy treated by the Perdew-Wang 91 parametrizations of the generalized gradient approximation (GGA) [20–22].

These QMD simulations are performed in the canonical (*NVT*) ensemble with fixed number of particles, volume, and temperature [23]. The density and temperature ranges are selected as $0.2 \sim 2.3$ g/cm^3 and $1000 \sim 80\,000$ K, respectively, with a typical helium mass fraction of 0.245 (220 hydrogen and 18 helium atoms) to highlight the interior conditions of Jupiter and Saturn. We fix the plane-wave cutoff at 1200 eV and use only the Γ point to sample the Brillouin zone in MD simulations. A sufficient number of bands are included to ensure the occupation of the highest band to a level of 10^{-5}. Through additional convergence tests for the particle number, the plane-wave cutoff and k-point Brillouin sampling are performed at several P-T conditions, both the internal energy and the pressure are confirmed to achieve good convergence. The trajectories evolve for 20 000∼30 000 steps with a time step of $0.3 \sim 0.6$ fs. These trajectories provide a consistent set of static, dynamic, and transport properties of the H-He mixtures.

B. Electrical and optical properties

To calculate the electrical and optical properties, we draw 10–15 configurations from the equilibrated portion of the MD run. For each configuration, we use a $4 \times 4 \times 4$ Monkhorst-Pack scheme k points to guarantee the energy convergence with higher precision [24]. Based on the quasi-independent particle approximation, the Kubo-Greenwood formula could estimate the real component of the frequency-dependent conductivity [25,26]:

$$\sigma_1(\omega) = \frac{2\pi}{3\omega\Omega}\sum_{\mathbf{k}} w(\mathbf{k}) \sum_{j=1}^{N}\sum_{i=1}^{N}\sum_{\alpha=1}^{3}[f(\epsilon_i,\mathbf{k}) - f(\epsilon_j,\mathbf{k})] \times |\langle\Psi_{j,\mathbf{k}}|\nabla_\alpha|\Psi_{i,\mathbf{k}}\rangle|^2 \delta(\epsilon_{j,\mathbf{k}} - \epsilon_{i,\mathbf{k}} - \hbar\omega), \quad (1)$$

where ω is the frequency, Ω is the atomic volume, and n is the total number of bands used. $\Psi_{i,\mathbf{k}}$ and $\epsilon_{i,\mathbf{k}}$ are the electronic eigenstates and eigenvalues for the electronic state i at $\mathbf{k}$, $f(\epsilon_i,\mathbf{k})$ stands for the Fermi distribution function, and $w(\mathbf{k})$ represents the $\mathbf{k}$-point weighting factor. The dc conductivity is obtained as the zero frequency limit of σ_1 by fitting it with the generalized Drude-Smith model [27]. The imaginary part of the frequency-dependent conductivity is related to $\sigma_1(\omega)$ through the Kramer-Krönig relation $\sigma_2(\omega) = -\frac{2}{\pi}\mathrm{P}\int \frac{\sigma_1(\nu)\omega}{(\nu^2-\omega^2)}d\nu$. The reflectivity is determined by

$$R(\omega) = \frac{[1-n(\omega)]^2 + k(\omega)^2}{[1+n(\omega)]^2 + k(\omega)^2}, \quad (2)$$

with the real and imaginary parts of refraction indices $[n(\omega),k(\omega)]$. which can be derived from the complex dielectric function by the relation of $\epsilon(\omega) = \epsilon_1(\omega) + i\epsilon_2(\omega) = [n(\omega) + ik(\omega)]^2$. The dielectric functions, in turn, follow immediately from the complex conductivity.

C. Transport properties

The self-diffusion coefficient D_α for species α is computed by the velocity autocorrelation function [28,29]

$$D_\alpha = \frac{1}{3}\int_0^\infty \langle \mathbf{V}_i(t)\cdot\mathbf{V}_i(0)\rangle dt, \quad (3)$$

with $\mathbf{V}_i$ being the velocity of the ith particle of species α. To derive this quantity for both H and He, we generate MD trajectories of sufficient temporal length to ensure the convergence of the integral. We also derive the mutual-diffusion coefficient $D_{\alpha\beta}$ according to the Green-Kubo relation [25,30,31]

$$D_{\alpha\beta} = \frac{Q}{3Nx_\alpha x_\beta}\int_0^\infty \langle A(t)A(0)\rangle dt, \quad (4)$$

where

$$A(t) = x_\beta\sum_{i=1}^{N_\alpha}\mathbf{V}_i(t) - x_\alpha\sum_{j=1}^{N_\beta}\mathbf{V}_j(t). \quad (5)$$

In the present study, the thermodynamic factor Q in Eq. (4) is chosen to be unity, the value for mixtures of ideal gases, as done in many other systems and conditions. x_α and N_α represent the concentration and particle number of species α, respectively.

The viscosity is computed from the autocorrelation function of the five off-diagonal components of the stress tensor [P_{xy}, P_{yz}, P_{zx}, $(P_{xx} - P_{yy})/2$, and $(P_{yy} - P_{zz})/2$] [32]

$$\eta = \lim_{t\to\infty}\overline{\eta}(t),$$

with

$$\overline{\eta}(t) = \frac{V}{k_B T}\int_0^t \langle P_{12}(0)P_{12}(t')\rangle dt'. \quad (6)$$

It should be noted that to obtain similar statistical accuracy, the viscosity and mutual diffusion require much longer trajectories than the self-diffusion coefficient because the single-particle correlations are averaged over the particles and gain significant statistical improvement. It has been found that empirical fits [33] to the integrals of the autocorrelation functions can substantially shorten the length of the trajectory required. And then the basic dynamic properties can be determined effectively by extrapolating the fits of the functional form $A[1 - \exp(t/\tau)]$ to $t \to \infty$ with A and τ the free parameters. Fitting to this form at short-time integrations produces reasonable approximations to η and $D_{\alpha\beta}$. In the present work, we generally fit over the interval $[0, 4\tau$–$5\tau]$. The fractional statistical error in computing a correlation function C for MD trajectories is estimated as $\Delta C/C = \sqrt{2\tau/T_{\mathrm{traj}}}$, in which T_{traj} is the length of the trajectory and τ is the correlation time of the function [34].

III. RESULTS AND DISCUSSION

To characterize the behavior of the H-He mixed plasmas at extreme conditions, the effective ionic coupling parameter Γ_{eff}

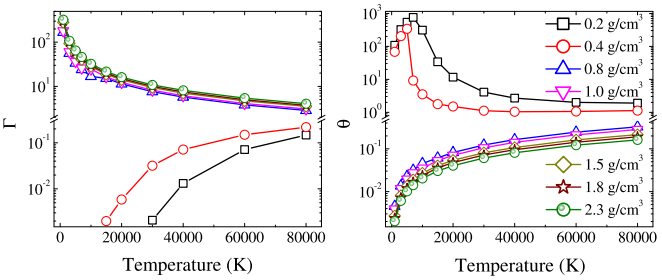

FIG. 1. (Color online) Effective ionic coupling parameter $\Gamma_{\rm eff}$ and the electron degeneracy parameter θ for H-He mixtures as functions of temperature at different densities.

and electron degeneracy parameter θ are introduced [35,36], namely,

$$\Gamma_{\rm eff} = \sum_i X_i \Gamma_i = \langle Z^{5/3} \rangle \langle Z \rangle^{1/3} \Gamma \tag{7}$$

and

$$\theta \equiv k_B T / E_f, \tag{8}$$

where $\langle Z \rangle$ represents the average ionization of the mixture, which is calculated using an average-atom model. $X_i = n_i/n$ denotes the mole fraction of species i (here, i = H, He), and $\Gamma \equiv e^2/(4\pi\epsilon_0 r_s k_B T)$ is the electron-electron coupling parameter with the Wigner-Seitz radius of the system given by $r_s = (\frac{4}{3}\pi n)^{-1/3}$, and the Fermi energy is expressed as $E_f \equiv \frac{\hbar^2}{2m_e}(3\pi^2 n_e)^{2/3}$, with n and n_e denoting the total number density of ions and electrons, respectively. The effective ionic coupling and the electron degeneracy parameters for the studied dense plasma are shown in Fig. 1. The plasma states are divided into two parts: the one is for the cases of 0.2 and 0.4 g/cm^3, lying in weak coupled ($\Gamma_{\rm eff} \ll 1$) and low degenerated state ($\theta \gg 1$); for the other cases, the ions are strongly or even moderately coupled ($\Gamma_{\rm eff} \geqslant 1$), and the electrons are highly or partially degenerated ($\theta \leqslant 1$). These two distinct kinds of ionic coupling and electron degenerate behavior come from the different ionization behaviors of H-He mixture at these conditions. The system is partially ionized at lower densities of 0.2 and 0.4 g/cm^3; while with increasing densities, the system becomes a fully ionized plasma, which will be discussed below. In the following, we focus on the EOS and structural and transport properties of H-He mixtures with typical helium mass fractions of 0.245 in these whole regimes.

A. Equations of state

Accurate EOS data of H-He mixtures are necessary to answer the fundamental questions about or make models regarding the composition and formation of planets. The EOSs of mixtures are usually determined by application of mixing rules in most of the modelings. However, the important effects of H-He demixing at high pressures cannot be explained with simple mixing rules. And thus more and more studies resort to the real mixture, especially by using the FT-DFT-based QMD method, which has been proven a successful tool to calculate the properties of complex plasmas under extreme conditions.

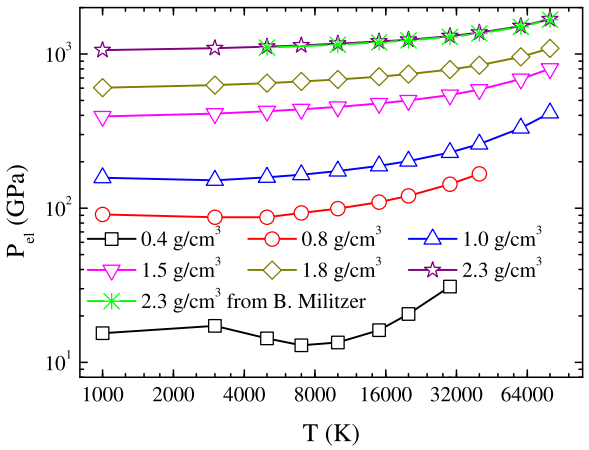

FIG. 2. (Color online) Electronic pressure of H-He mixtures as a function of temperature for different densities. For comparison, the results from Militzer are also included [39].

The pressure of H-He mixtures can be expressed as

$$P_{\rm tot} = P_{\rm el} + P_{\rm ion}, \tag{9}$$

where $P_{\rm el}$ evaluates the electronic pressure part using the force provided by VASP, which contains contributions from the direct ion-ion interaction and a term from the gradient of the electronic total energy. The ionic pressure part $P_{\rm ion}$ comes from the ideal gas expression since the ions move classically [37,38]. Thus it is expressed as $P_{\rm ion} = nk_B T$ with n the total ion number density.

The electronic pressures of H-He mixtures derived from the QMD simulations are displayed in Fig. 2, which could describe various transient processes such as dissociation or association of chemical bonds and ionization or recombination induced by temperature or density without any approximation. For comparison, we also include the results from Militzer, which take into account the nuclear quantum effects [39]. As shown in Fig. 2, our results agree well with those from Militzer [39], indicating that the nuclear quantum effects become unimportant in the relevant conditions. In addition, a liquid-liquid phase transition is found at lower temperatures, which is characterized by the negative slope of $P_{\rm el}$ with respect to temperature at constant density. This is attributed to the molecular dissociation. However, we do not find any signs of plasma phase transition ($\frac{\partial P_{\rm el}}{\partial V}|_T > 0$), which is characterized by the abrupt electronic ionization.

In the following, the ionizations of both H and He are considered. We evaluate the ionization degree of H and He in the mixture based on an average-atom (AA) model [40], which solves the Hartree-Fock-Slater equation in a self-consistent field approximation assuming a finite temperature. As an illustration, we plot in Fig. 3 the average ionizations of H and He in H-He mixtures as functions of density at different temperatures. For lower densities below 0.5 g/cm^3, the H-He system could be described as a partially ionized plasma. As the density is increased, the system becomes a fully ionized plasma.

The total pressures of H-He mixtures including the two parts of contributions are plotted as functions of temperature at different densities in Fig. 4, along with the demixing lines from

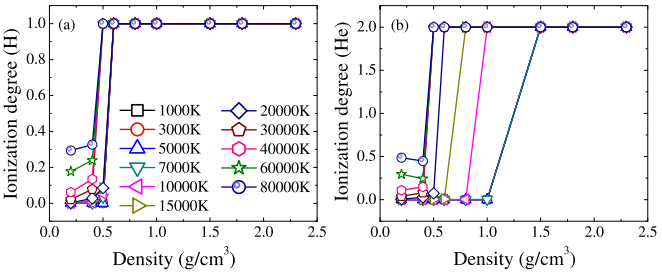

FIG. 3. (Color online) Ionization degrees of (a) H and (b) He as functions of density for different temperatures.

Morales *et al.* [11,12]. All of the pressures show a systematic tendency to increase with temperature at these densities. It can be seen that some of our considered conditions fall into the demixing regime. In the following, we focus on the effects of demixing on the structural, electronic, and transport properties in these regimes.

B. Structural properties and phase separation

We reexamine the phase separation of H-He mixture in the region bordered with the demixing lines from Morales *et al.* [11,12] using QMD simulations. Soubiran *et al.* have reported a direct observation of H-He demixing in MD simulations with much higher helium concentrations [14]. Recently, Militzer confirmed that the demixing occurs at about 1.1 g/cm^3 and 3000 K with the relative lower helium mass fraction as the one we use [39]. We pay attention to studying the cases at higher densities and temperatures. Figures 5(a) and 5(b) present the trajectories of H and He atoms over 200 time steps at 1.8 g/cm^3 for 5000 K and 10 000 K, respectively. It is obvious that these two cases are quite distinct from each other. The system separates into helium-rich and hydrogen-rich phases at 5000 K, while at 10 000 K the trajectories are delocalized and the system is in a mixed state. To clarify the structural change of the system, we calculate the pair distribution functions (PDFs) of each pair of atom types, which give the possibility of finding an atom of a given

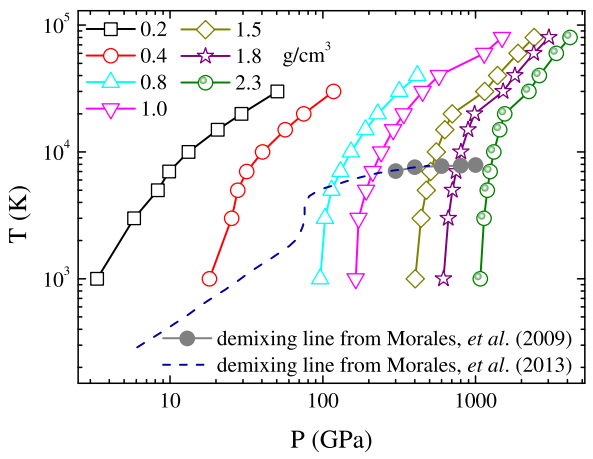

FIG. 4. (Color online) Total pressures of H-He mixtures as functions of the temperature at different densities, along with the demixing lines from Morales *et al.* [11,12].

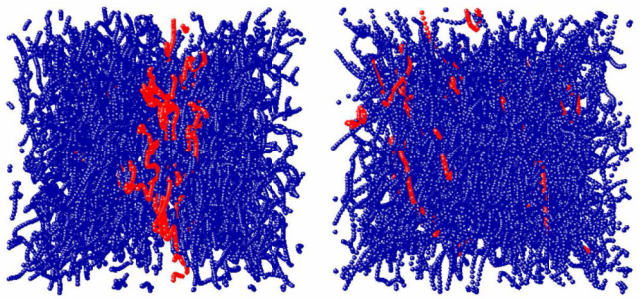

FIG. 5. (Color online) Trajectories of H and He atoms over 200 time steps at 1.8 g/cm^3 for 5000 K and 10 000 K.

type at a given distance from a reference atom. The results are presented in Fig. 6. As the temperature decreases from 10 000 K to 5000 K, the peaks of $g_{\text{H-H}}$ and $g_{\text{He-He}}$ rise, while the H-He peak is reduced. In addition, $g_{\text{He-He}}$ drops below 1 at larger distances. All of these signatures indicate that the phase separation takes place at 5000 K for 1.8 g/cm^3.

Furthermore, we gain insight into the dissociation of hydrogen for H-He mixtures by calculating the coordination number of H, which is a weighted integral over the PDFs $g(r)$ of H-H,

$$K(r) = \frac{N-1}{V}\int_0^r 4\pi r'^2 g(r')\,dr'. \tag{10}$$

The fraction of the ions bounded to a hydrogen molecule is twice the value of $K(r)$ at the first peak in $g(r)$. As shown in Fig. 7, for the density and temperature state of 0.4 g/cm^3 and 1000 K the PDF of H-H peaks at about 0.73 Å, which corresponds to the bond distance of the hydrogen molecule in the H-He mixture. The molecular peak in the PDF of H-H in pure hydrogen has been reported to be about 0.748 Å. This means that the effect of helium on hydrogen in H-He mixtures is to shorten the bond distance and thus make the hydrogen molecules more stable. As the density and temperature increase, the hydrogen molecules dissociate with the significant reduction and broadening of the maxima of $g(r)$, with the dissociation degree about 71% at 0.8 g/cm^3 and 5000 K.

C. Electrical and optical properties

Figures 8(a) and 8(b) show the isotherms and isochores of dc electrical conductivity over a wide range of densities and temperatures, respectively. The conductivity rises systematically with increasing density in the whole range we studied, which results from the increase of conducting electrons due to pressure ionization. Similar to that in pure hydrogen [41], the feature of the liquid-liquid phase transition for the H-He mixture could be identified by the fact that the conductivity is increased over several orders of magnitude in a small density interval at low temperatures from 1000 to 5000 K. In addition, the isochores clearly show that the conductivity decreases for temperatures above 5000 K and densities higher than 1.0 g/cm^3, which signifies the nonmetal-metal transition of the H-He mixture. At lower densities, the rising conductivity

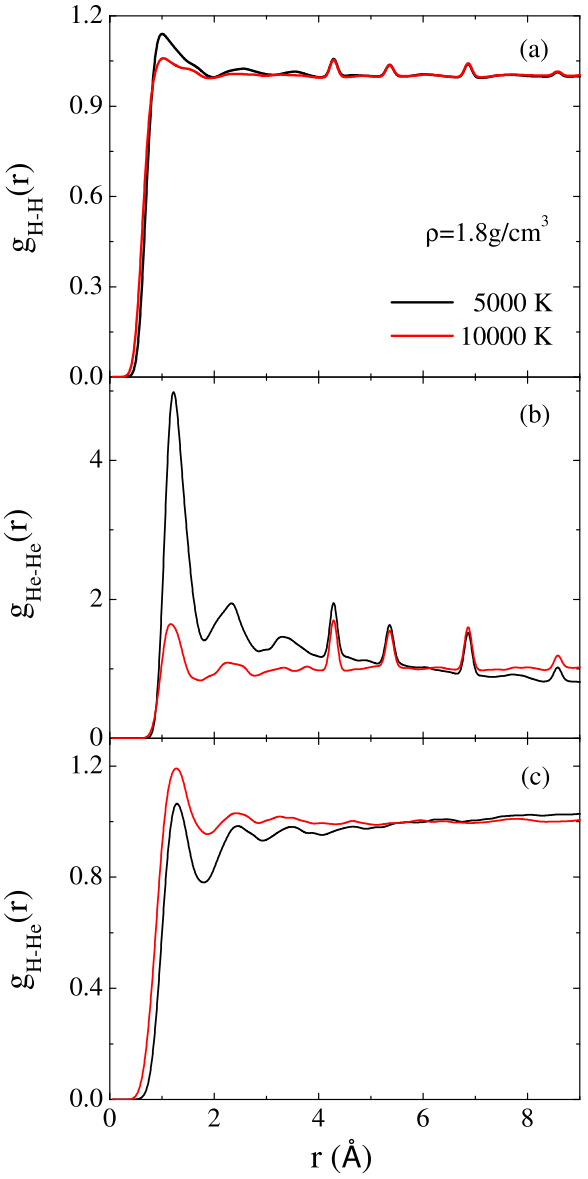

FIG. 6. (Color online) Pair distribution functions for (a) H-H, (b) He-He, and (c) H-He at 5000 (black line) and 10 000 (red or gray line) K for 1.8 g/cm^3.

with increasing temperature comes from thermal ionization. For the whole temperature range, the conductivity generally rises with increasing density.

In Fig. 9, the behavior of the absorption spectra at four different densities of 0.2, 0.4, 1.5, and 2.3 g/cm^3 along different isotherms is presented. It is demonstrated that as the temperature increases, the absorption spectra exhibit a nearly free-electron nature, with the peak locating at the plasma frequency. With the density increasing, the peak shifts to higher energy. The feature of absorption discontinuity appears for the plots at relatively low temperatures of 1000 and 3000 K for densities of 0.2 and 0.4 g/cm^3, which could be explained by analyzing the electronic density of states (DOS) shown in Fig. 10. It can be seen that the DOS at 3000 K for densities of 0.2 and 0.4 g/cm^3 exhibits a gap of about 5.23 and 2.59 eV, respectively, corresponding to

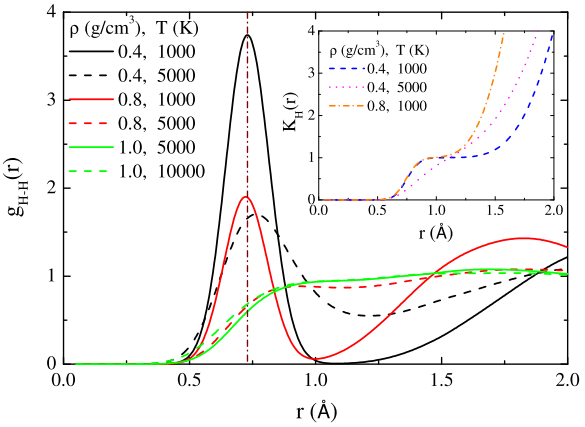

FIG. 7. (Color online) Pair distribution functions for H-H at different densities and temperatures. The inset shows the coordination numbers of H at different densities and temperatures.

the locations of the absorption discontinuity. This suggests that the small absorption before the jump comes from the intraband transition. As the temperature increases, the gap is closed and thus the absorption spectrum becomes smooth. At higher densities, the absorption presents systematic behavior corresponding to the collective excitation.

D. Diffusion and viscosity properties

We used QMD simulations to calculate the diffusion and viscosity coefficients of H-He mixtures in the strong coupling regime (the corresponding density and temperature ranges are 0.8–2.3 g/cm^3 and 1000–30 000 K), without making binary collision approximations as in the plasma models. By fitting the QMD results using the empirical formula, the self- and mutual-diffusion coefficients, as well as the viscosity, are obtained with the correlation time between 5 and 20 fs. A total uncertainty of $\backsim$20% in mutual diffusion coefficient and viscosity comes from the fitting and extrapolation to infinite time, while the error in the self-diffusion coefficient is less than 1% due to an additional average over the particles. To compare the self-diffusion coefficient calculated by QMD with the one-component-plasma (OCP) model conveniently, it is reduced to a dimensionless form: $D_j^* = D_j/\omega_p a^2$ for the two ionic species j = H, He, where $\omega_p = (4\pi n/\varepsilon_0\langle m\rangle)^{1/2}\langle Z\rangle e$ is the mixed plasma frequency. In Fig. 11(a), we present the reduced self-diffusion coefficients for H and He as functions of the ionic

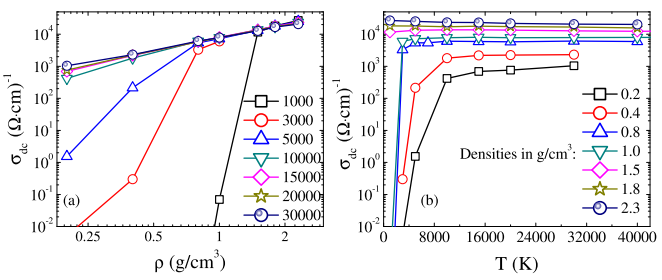

FIG. 8. (Color online) Electrical conductivity in dense H-He mixtures as a function of (a) density for different temperatures and (b) temperature for different densities.

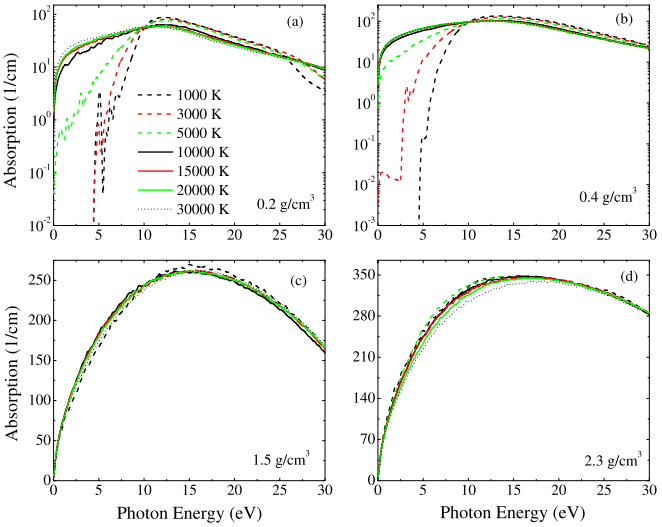

FIG. 9. (Color online) Absorption coefficient of H-He mixtures at different densities along different isotherms.

coupling parameter, along with the results from OCP [35,42] and Yukawa (with $\kappa = 0.1$) [43] models for comparison. The present results from QMD show visible divergence with those from OCP and Yukawa models. Even the best accordance between our D^*_H and the fitting formula of Hansen *et al.* [44] ($D^* = 2.95\Gamma^{-1.34}$) yields a difference of about $5\% \backsim 50\%$. This is because the QMD results come from the real mixture, while the other models are restricted to the one component and fully ionized plasma. In the strongly coupling regime, Daligault proposed an empirical law [$D^*_j = \frac{A_j}{\Gamma}\exp(-B_j\Gamma)$] to describe the diffusion process based on the cage model, and extended this approach for OCP to binary ionic mixtures by the use of $\Gamma_{\rm eff}$ and the mixed plasma frequency [36]. We fit the present reduced self-diffusion coefficient for H and He using the empirical law, as shown in Fig. 11(b). The fitting parameters are $A_{\rm H} = 1.0765$, $B_{\rm H} = 0.00975$; $A_{\rm He} =$

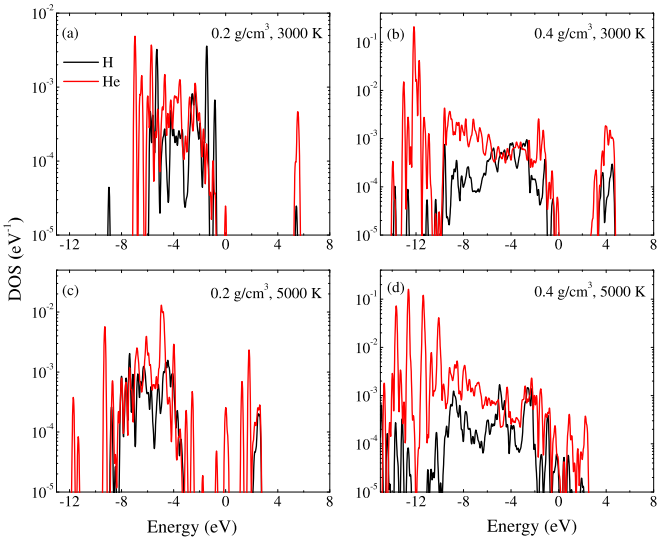

FIG. 10. (Color online) Density of states (DOS) of H-He mixtures at four density and temperature conditions.

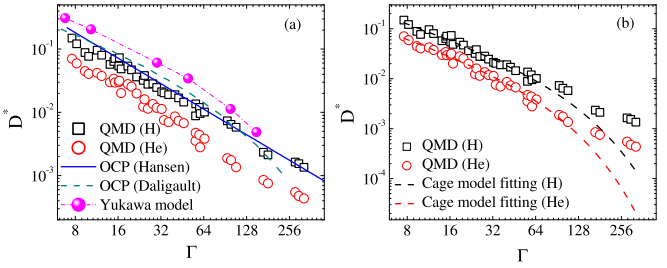

FIG. 11. (Color online) Reduced self-diffusion coefficients from QMD for H and He, along with (a) the previous results from OCP and Yukawa models and (b) the fitting data with the cage model.

0.5434, $B_{\rm He} = 0.0136$. It could be seen that our data follow the cage model very well at weaker coupling regions ($\Gamma \leqslant 64$), while they diverge at regions with stronger coupling, which just falls into the demixing regime at low temperature as mentioned above. As an important part of mixing, diffusion is surely to be affected by the demixing of the H-He mixture. And therefore, the QMD simulations could capture not only the many-body effects but also the demixing of the mixture governing the diffusion. Empirical models are not expected to work well for the mixed hot dense plasmas.

Furthermore, we examine the behaviors of mutual diffusion and viscosity of H-He mixtures as functions of ionic coupling parameters at different densities, as shown in Fig. 12. It is indicated that the mutual-diffusion coefficient becomes a function of only the coupling parameter Γ. For $D_{\text{H-He}}$ the Γ range is split into two parts: $D_{\text{H-He}}$ decreases with Γ almost linearly for values of $\Gamma \leqslant 64$, exhibiting liquidlike behavior; a break with steeper slope shows up at the value of $\Gamma \backsim 64$, entering the H-He demixing regime. The mutual-diffusion is related to the collective transport of mass driven by the concentration gradient. At their respective local areas after demixing of H-He mixtures, the concentration fluctuations almost disappear, and the mutual-diffusion coefficients become very small. However, based on Fick's law, the steep composition gradient at the interface should induce the intermixing of the different components. The stable existence of the phase separation demonstrates that the diffusion at these regimes exhibits some non-Fickian effects. The viscosity of the H-He mixture has a complex behavior under extreme conditions, resulting from two competitive mechanisms of the bodily movement of particles and the action of interparticle forces at a distance. At the coupling region of $7 \leqslant \Gamma \leqslant 50$, the contributions from

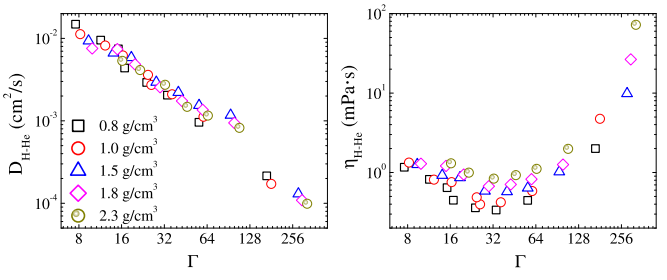

FIG. 12. (Color online) Mutual-diffusion and viscosity coefficients of H-He mixtures as functions of ionic coupling for different densities.

the two mechanisms are almost similar, and thus lead to a shallow minimum near $\Gamma \backsimeq 33$. At larger coupling, the viscosity increases with increasing ionic coupling, that is, increasing density (or lowering temperature), satisfying the Arrhenius-type relation [45].

The well-known Stokes-Einstein relation provides a connection between self-diffusion and shear-viscosity coefficients of dense fluids as $\frac{D\eta}{k_B T n_i^{1/3}} = C_{\mathrm{SE}}$, with C_{SE} a constant. Chisolm and Wallace have proposed an empirical value of 0.18 ± 0.02 from a theory of liquid near melting [46]. It has been reported that the Stokes-Einstein expression for Be holds the general feature of liquids as predicted by Chisolm and Wallace in the strong coupling region [47]. We extend such a relation for single species to the mixture. The Stokes-Einstein–like expression between mutual-diffusion and viscosity coefficients are established, as shown in Fig. 13. It is noted that similar to that in the one-component Be plasma, the Stokes-Einstein behavior first increases with temperature in the region of $7 \leqslant \Gamma \leqslant 21$, and then keeps almost constantly close to the Chisolm-Wallace value during the range from 21 to 64. This transition suggests the change from a kinetics-dominated to a potential-dominated regime. However, an obvious different behavior appears when it departs from the constant value at large values of $\Gamma > 64$. This should be induced by the H-He demixing process.

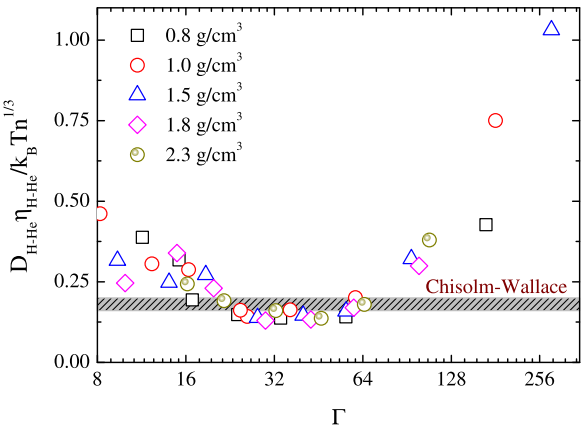

FIG. 13. (Color online) Examination of the Stokes-Einstein–like relation between mutual-diffusion and viscosity coefficients of H-He mixtures along the coupling parameter for different densities. The Chisolm-Wallace predicted value is denoted by the light-gray region [46].

IV. SUMMARY

In conclusion, the complex behavior of H-He mixtures at extreme conditions relevant to giant planet interiors has been explored comprehensively. The EOSs suggest the occurrence of the liquid-liquid phase transition of H at lower temperatures. We examined H-He demixing through structural analysis. The dc conductivities at wide temperature-density ranges were determined in combination with Kubo-Greenwood formula. It was noted that the absorption discontinuity feature exists at lower temperatures for low densities, which comes from the change from intraband to interband transition at the semiconducting regime. The self- and mutual-diffusion coefficients are strongly affected by H-He demixing, even including some non-Fickian effects. We found that the Stokes-Einstein–like relation exists between the mutual-diffusion and viscosity coefficients, and at larger coupling, the relation diverges from a constant because of the demixing.

ACKNOWLEDGMENTS

This work was supported by NSFC under Grants No. 11205019, No. 11474034, and No. 11275032, and by the Foundations for Development of Science and Technology of China Academy of Engineering Physics under Grant No. 2015B0102022.

[1] M. Podolak and R. T. Reynolds, Icarus **46**, 40 (1981).
[2] W. B. Hubbard, T. Guillot, M. S. Marley, A. Burrows, J. I. Lunine, and D. S. Saumon, Planet. Space Sci. **47**, 1175 (1999).
[3] S. Atzeni and J. Meyer-ter-vehn, *The Physics of Inertial Fusion: Beam Plasma Interaction, Hydrodynamics, Hot Dense Matter*, International Series of Monographs on Physics (Clarendon, Oxford, 2004).
[4] J. D. Lindl, *Inertial Confinement Fusion: The Quest for Ignition and Energy Gain Using Indirect Drive* (Springer, New York, 1998).
[5] Y. J. Gu, Q. F. Chen, L. C. Cai, Z. Y. Chen *et al.*, J. Chem. Phys. **130**, 184506 (2009).
[6] R. Smoluchowski, Nature (London) **215**, 691 (1967).
[7] D. J. Stevenson and E. E. Salpeter, Astrophys. J. Suppl. Ser. **35**, 239 (1977).
[8] D. J. Stevenson and E. E. Salpeter, Astrophys. J. Suppl. Ser. **35**, 221 (1977).
[9] J. E. Klepeis, K. J. Schafer, T. W. Barbee, III, and M. Ross, Science **254**, 986 (1991).
[10] O. Pfaffenzeller, D. Hohl, and P. Ballone, Phys. Rev. Lett. **74**, 2599 (1995).
[11] M. A. Morales, E. Schwegler, D. M. Ceperley, C. Pierleoni, S. Hamel, and K. Caspersen, Proc. Natl. Acad. Sci. USA **106**, 1324 (2009).
[12] M. A. Morales, S. Hamel, K. Caspersen, and E. Schwegler, Phys. Rev. B **87**, 174105 (2013).
[13] W. Lorenzen, B. Holst, and R. Redmer, Phys. Rev. Lett. **102**, 115701 (2009).
[14] F. Soubiran, S. Mazevet, C. Winisdoerffer, and G. Chabrier, Phys. Rev. B **87**, 165114 (2013).
[15] C. Wang, X. T. He, and P. Zhang, Phys. Rev. E **88**, 033106 (2013).
[16] G. Kresse and J. Hafner, Phys. Rev. B **47**, 558 (1993).
[17] G. Kresse and J. Fürthmuller, Phys. Rev. B **54**, 11169 (1996).
[18] T. J. Lenosky, S. R. Bickham, J. D. Kress, and L. A. Collins, Phys. Rev. B **61**, 1 (2000).
[19] S. Bagnier, P. Blottiau, and J. Clérouin, Phys. Rev. E **63**, 015301(R) (2000).

[20] G. Kresse and D. Joubert, Phys. Rev. B **59**, 1758 (1999).
[21] P. E. Blöchl, Phys. Rev. B **50**, 17953 (1994).
[22] J. P. Perdew, P. Ziesche, and H. Eschrig, *Electronic Structure of Solids'91* (Akademie Verlag, Berlin, 1991).
[23] S. Nosé, J. Chem. Phys. **81**, 511 (1984).
[24] H. J. Monkhorst and J. D. Pack, Phys. Rev. B **13**, 5188 (1976).
[25] R. Kubo, J. Phys. Soc. Jpn. **12**, 570 (1957).
[26] D. A. Greenwood, Proc. Phys. Soc. London **71**, 585 (1958).
[27] N. V. Smith, Phys. Rev. B **64**, 155106 (2001).
[28] J. Hansen and I. McDonald, *Theory of Simple Liquids* (Elsevier, New York, 2006).
[29] N. March and M. Tosi, *Atomic Dynamics in Liquids*, Dover Books on Physics and Chemistry (Dover, New York, 1991).
[30] R. Kubo, M. Yokota, and S. Nakajima, J. Phys. Soc. Jpn. **12**, 1203 (1957).
[31] R. Zwanzig, J. Chem. Phys. **40**, 2527 (1964).
[32] M. P. Allen and D. J. Tildesley, *Computer Simulation of Liquids* (Oxford University, Oxford, 1987).
[33] J. D. Kress, James S. Cohen, D. P. Kilcrease, D. A. Horner, and L. A. Collins, Phys. Rev. E **83**, 026404 (2011).
[34] R. Zwanzig and N. K. Ailawadi, Phys. Rev. **182**, 280 (1969).
[35] J. P. Hansen, G. M. Torrie, and P. Vieillefosse, Phys. Rev. A **16**, 2153 (1977).
[36] J. Daligault, Phys. Rev. Lett. **108**, 225004 (2012).
[37] B. Holst, R. Redmer, and M. P. Desjarlais, Phys. Rev. B **77**, 184201 (2008).
[38] L. A. Collins, J. D. Kress, and D. E. Hanson, Phys. Rev. B **85**, 233101 (2012).
[39] B. Militzer, Phys. Rev. B **87**, 014202 (2013).
[40] A. F. Nikiforov and V. G. Novikov, *Quantum-statistical Models of Hot Dense Matter: Methods for Computation Opacity and Equation of State* (Springer, Berlin, 2000).
[41] B. Holst, M. French, and R. Redmer, Phys. Rev. B **83**, 235120 (2011).
[42] J. Daligault, Phys. Rev. Lett. **96**, 065003 (2006).
[43] $\kappa = k_D a$ is a dimensionless parameter with k_D^{-1} the screening length and a the interparticle distance.
[44] J. P. Hansen, I. R. McDonald, and E. L. Pollock, Phys. Rev. A **11**, 1025 (1975).
[45] M. Dyer, C. Zhang, and A. Alavi, ChemPhysChem **6**, 1711 (2005).
[46] E. Chisolm and D. Wallace, in *Shock Compression of Condensed Matter - 2005*, AIP Conf. Proc. No. 845, edited by M. D. Furnish, M. Elert, T. P. Russell, and C. T. White (AIP, New York, 2006).
[47] C. Wang, Y. Long, M. F. Tian, X. T. He, and P. Zhang, Phys. Rev. E **87**, 043105 (2013).